ELSEVIER

Surface and Coatings Technology 90 (1997) 6–13

SURFACE & COATINGS TECHNOLOGY

Oxidation improvement of Ti–48Al–2Cr–2Nb intermetallics by air plasma sprayed ZrO_2–Ni–4.5wt.%Al coatings

I.C. Hsu, S.K. Wu *

Institute of Materials Science and Engineering, National Taiwan University, Taipei, Taiwan 106, ROC

Received 22 February 1996; accepted 15 July 1996

Abstract

The air plasma spraying (APS) technique was employed to modify the oxidation resistance of Ti–48Al–2Cr–2Nb intermetallics. The Ni–4.5wt.%Al bond-coat provided a good bonding strength between matrix and thermal barrier top-coat. Static and thermal cyclic tests showed improvement in oxidation resistance of APS-coated Ti–48Al–2Cr–2Nb alloy although the oxidation kinetics did not obey the parabolic law. The oxidation rate was reduced by the formation of NiO scale on the outer layer of the bond-coat which slowed down the oxygen permeation. It was healed by the formation of an Al_2O_3 layer in the inner layer of the bond-coat which can prevented outward diffusion of titanium. A Ti–Al–Ni inter-diffusional layer was observed in between the bond-coat and the matrix. A mechanism of oxidation protection by APS coatings is therefore proposed in this study.

Keywords: Oxidation; Intermetallics; Air plasma spraying

1. Introduction

TiAl intermetallics are potentially good high-temperature materials because of their high modulus retention and good creep resistance characteristics at elevated temperatures [1–3]. However, low ductility at room temperature and insufficient oxidation resistance at high temperatures restrict their applications [4,5]. Among all titanium aluminides, γ-titanium aluminides are the most popular ones because of their higher specific strength and better mechanical properties. In order to further improve the mechanical properties, binary γ-titanium aluminides have been modified by Nb and Cr. One example is the Ti–48Al–2Cr–2Nb alloy (in at.%) [6]. This modified titanium aluminide exhibits good high-temperature strength as well as corrosion resistance, however, it still lacks cyclic oxidation protection at temperatures beyond 1000°C [7]. Air plasma spraying (APS) processes have been employed commercially for about 20 years [8–10]. This process represents a convenient and rapid method for providing a protection layer at high temperature. The APS-ZrO_2 coating is an effective process to prevent oxidation of superalloys [11–13].

Basically, APS is used for improving the wear resistance and chemical stability at elevated temperatures for the moving parts of refractory metallic components. Mechanical bonding between the coatings and matrix materials is built up during the spraying process. A single layer or multi-layer of refractory ceramics or alloys is sprayed on the surface of base alloys. In order to increase the bonding strength, in addition to mechanical bonding, the surface of base alloy is usually activated by spraying a layer of bond-coat prior to the deposition of the top-coat. The design of bond-coat materials improved gradually, from using single nickel powder (simply by surface activation) to the development of Ni + x%Al powder until the modern MCrAlY powders were developed, which perform dual functions: surface activation and corrosion protection.

The application of APS to modify the surface of Ti–48Al–2Cr–2Nb intermetallics has not been reported in previous literature. The purpose of this work is to investigate the feasibility of extending the APS technique to the modification of intermetallic compounds. A Ni–4.5wt.%Al powder has been selected as the bond-coat material for two purposes. First, it was expected that there would be a good compatibility between bond-coat and matrix because aluminum is a common element in both. Second, it is helpful to identify the major role for nickel and aluminum in bond-coats for oxidation protection. In this study, an APS–ZrO_2 coating process with Ni–4.5wt.%Al as a bond-coat was used to modify

* Corresponding author.

PII S0257-8972(96)03032-0

the oxidation resistance of a Ti–48Al–2Cr–2Nb specimen. The oxidation characteristics of APS coating layers, and the reasons why these coating layers can improve the oxidation resistance of Ti–48Al–2Cr–2Nb alloy are also discussed.

2. Experimental details

A conventional tungsten vacuum arc melting technique was employed to prepare the Ti–48Al–2Cr–2Nb (at.%) alloy. Titanium (purity, 99.7%), aluminum (purity, 99.97%), chromium (purity, 99.9%) and niobium (purity, 99.7%), totaling about 80 g were melted and remelted six times in a low-pressure argon atmosphere. The as-melted button was homogenized at 1200°C in a 7×10^{-5}-Torr vacuum furnace for 24 h and then followed by furnace cooling. The homogenized button was cut into $5 \times 5 \times 80$-mm specimens for the APS coating. The equipment for APS used in this study was from METCO, USA. A bond-coat layer of Ni–4.5wt.%Al and a top-coat layer of ZrO_2–8wt.%CaO (all METCO commercial products, with commercial names METCO-450 and METCO-210 powders, respectively) were sprayed on specimens under ambient air pressure. The plasma spraying conditions are shown in Table 1. Grit blasting was conducted to clean and activate the specimen surface. After APS, the specimens were examined by optical microscopy (OM), scanning electron microscopy (SEM), electron probe microanalysis (EPMA), X-ray diffraction (XRD), thermal gravitation analysis (TGA), and micro-Vickers hardness testing, to investigate the characteristics of coating layers. The oxidation behavior of APS specimens was tested by the static and thermal cycling methods in which a 1000°C tube furnace was used. The specimen size used for the thermal cycling test was $5 \times 5 \times 50$ mm. For each thermal cycle, the specimen was put into a 1000°C furnace for 20 min and then left to cool to room temperature for another 20 min. The weight gain of the oxidized specimen was measured using a balance after every five thermal cycles. The samples were then sectioned with a low speed diamond saw and mounted on edge to observe the cross-section by Nikon 104 OM and Philips 515 SEM+EDAX without etching. The EPMAs used in this study were JEOL JXA-8600SX and JEOL JXA-8621MX (color) operated at 15 kV with a beam current of 20 nA. The probe spot size was 1 μm and the counting time was 60 s. A Setaram TGA-92 system was used for the static oxidation analysis. The micro-Vickers hardness was tested with Akashi MVK-E *II* under 100 g loading and 15 s loading time. The XRD analysis was conducted using a Philips 1710 apparatus at 30 kV and 20 mA.

Table 1
Plasma spray conditions used in this study

Gas	N_2/H_2
Nozzle	type G
Gas pressure	50 psi
Gas flow	75 pts
Arc	500 A
	75 V
RPM (meter wheel)	45
Spray distance	60 mm
Spray rate	5.4 kg h^{-1}
Convergence	7.6 m^2 h^{-1} (0.1 mm)$^{-1}$
Powder weight	0.73 kg m^{-2} (0.1 mm)$^{-1}$
Deposit efficiency	75%

3. Results and discussions

3.1. Microstructure, XRD and hardness of as-APS specimens

The OM microstructures of APS specimens are shown in Fig. 1(a) and Fig. 1(b), at two magnifications. The thickness of the top-coat layer is about 400 μm and that

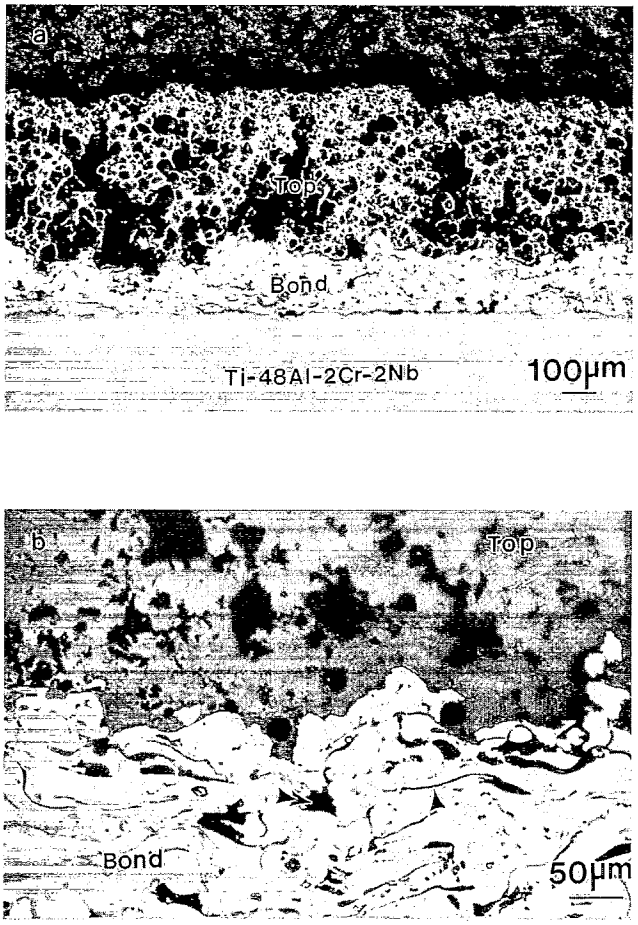

Fig. 1. OM microstructure shows (a) the interfaces between top-coat, bond-coat and matrix, and (b) the interface between top-coat and bond-coat.

of the bond-coat layer is about 200 μm. In Fig. 1(b), many voids are found in the black area of the top-coat layer, but very few voids can be observed in the bond-coat layer. The dark regions of the bond-coat layer are the un-mixed pure aluminum powder or other oxides which were formed during the plasma spraying process, as shown in Table 2, which gives the EPMA quantitative analysis of the bond-coat layer. As seen from Fig. 1(a) and Fig. 1(b), the interface between matrix and bond-coat is slightly rough, however, the interface between bond-coat and top-coat is much rougher. No crack is found at these two interfaces. The roughness at the interfaces provides them with a good mechanical bonding strength. Grit blasting before the APS can activate the specimen surface and provides additional good bonding at the interface of bond-coat and matrix.

It is well known that the bond-coat plays a very important role for plasma spraying, especially in the case of a plasma-sprayed ceramic coating on the surface of metals or superalloys. In order to understand if chemical bonding exists at the interface, the XRD spectra at the interface between bond-coat and matrix were investigated. The as-APS specimen was polished using emery paper to obtain a bond coat thickness of about 30 μm. Then the polished as-APS specimen was examined by XRD and the result is shown in Fig. 2. From Fig. 2, only the spectra of the Ti–48Al–2Cr–2Nb matrix and the Ni bond-coat are identified. Note that the Al peak is not prominent in Fig. 2. It is also notable that there is no indication of a chemical reaction at this interface. Obviously, the bonding force at the interface for the as-APS specimen is solely due to the mechanical bonding.

Fig. 1(a) shows that the top-coat of CaO stabilized ZrO_2 ceramics has a porous structure. Porous zirconium oxide is an excellent thermal barrier layer for heat gradient application [14]. It also exhibits a high degree of stability against chemical attack as well as corrosion protection. Fig. 3 shows the hardness vs. the depth position from the surface of the as-APS specimen. From Fig. 3, the hardness of APS coating has significantly improved due to the ZrO_2 coating, in spite of its porous structure. At the same time, the hardness of the top-coat layer is almost doubled in comparison with the titanium aluminide intermetallic matrix. This situation is very similar to that which occurred in the APS coating of Ni-based superalloys [15]. The inherently hard

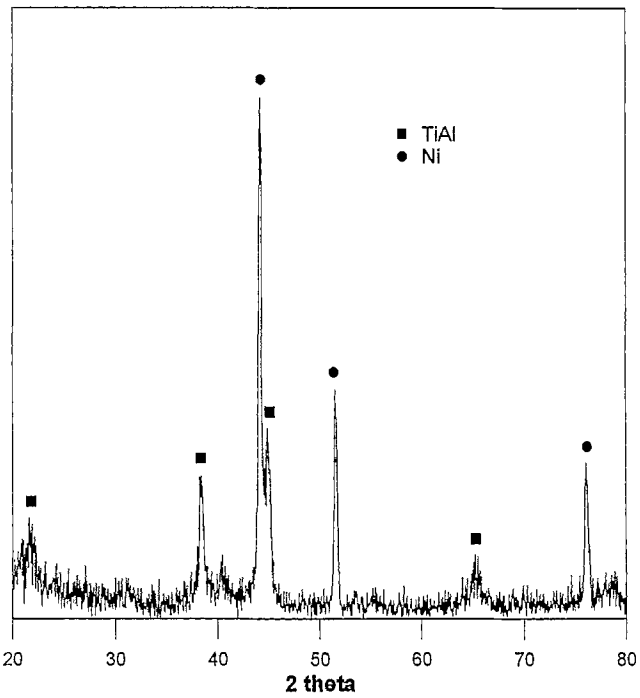

Fig. 2. XRD spectrum at the interface between bond-coat and matrix.

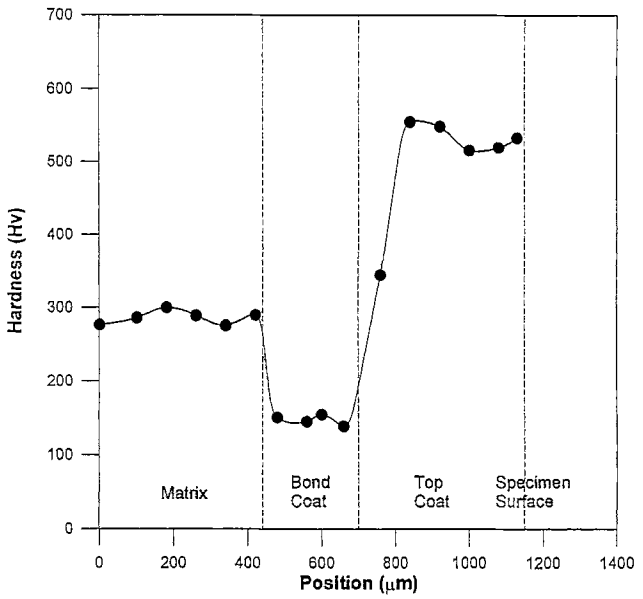

Fig. 3. Micro-hardness profile along the coating depth.

Table 2
EPMA quantitative analysis of the bond-coat layer

Detected area of the bond-coat layer	Ni (wt.%)	Al (wt.%)	O (wt.%)	Impurities (wt.%) (Zr, Ca, Fe, etc.)
Base alloy	Balance	4.3650	0.2010	<0.001
Dark planar streak (indicated by arrow)	<0.001	2.3861	20.6732	Balance
Dark large regions (indicated by double arrow)	<0.001	Balance	4.5582	<0.001

ZrO_2 ceramic coatings also have great potential due to their chemical inertness and wear resistance.

3.2. Oxidation tests of APS specimens

3.2.1. Static oxidation test and its kinetic behavior

In order to understand the oxidation resistance, the APS-coated Ti–48Al–2Cr–2Nb alloy was oxidized in air at 1000°C for different periods. Fig. 4 and Fig. 5 illustrate the secondary electron image (SEI), together with Ti and Al elements EPMA mapping of the un-coated (Fig. 4) and the coated (Fig. 5 with additional Ni-mapping) specimens, both oxidized at 1000°C for different lengths of time. (Nb and Cr elements were also conducted in the EPMA mapping but showed no significance.) From Fig. 4, for the un-coated Ti–48Al–2Cr–2Nb alloy, one can observe that severe

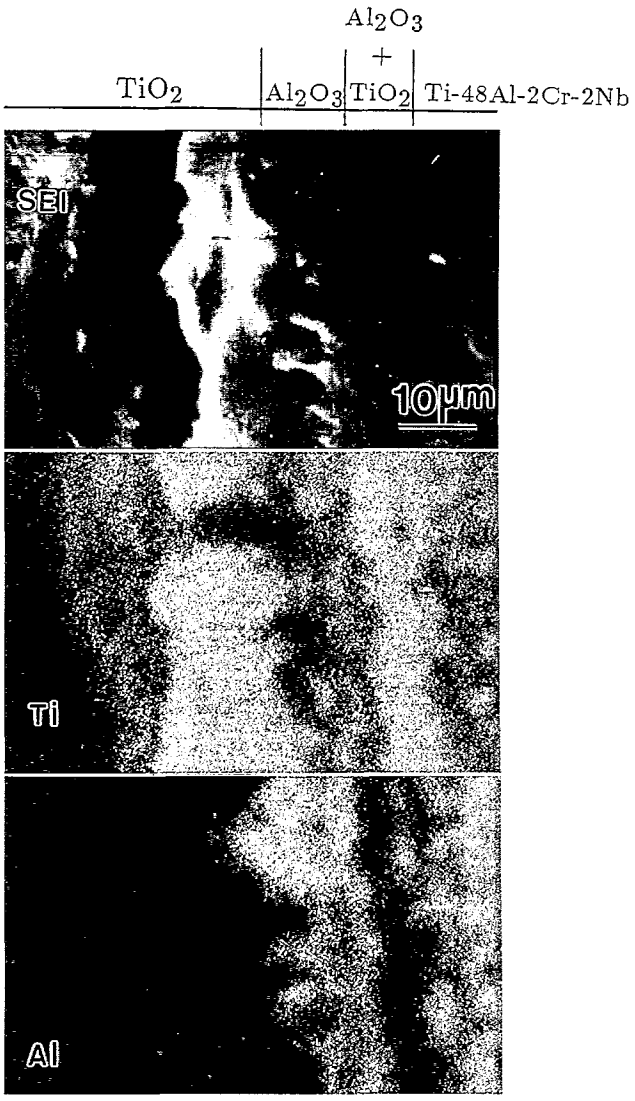

Fig. 4. SEI image and Ti and Al EPMA mappings of the un-coated specimen oxidized at 1000°C for 5 h.

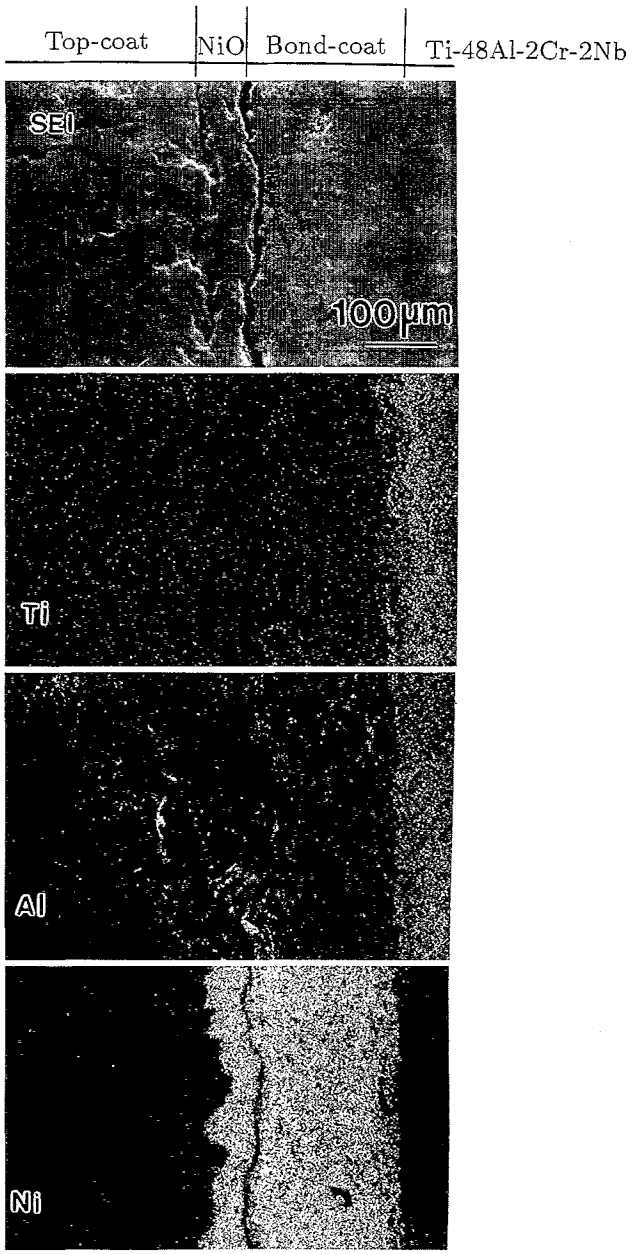

Fig. 5. SEI image and Ti, Al, and Ni EPMA mappings of the coated specimens oxidized at 1000°C for 27 h.

oxidation occurred at or beneath the specimen surface oxidized at 1000°C for 5 h. Scales of oxides TiO_2 and Al_2O_3 were formed on the surface. For the longer oxidation specimen, the oxygen can continue to diffuse into the unoxidized zone. The bonding strength between the oxidation scale layer and the unoxidized zone was found to be weak and easy to spall off. While, for the coated specimen, the oxidation situation is shown in Fig. 5 in which the specimen was oxidized at 1000°C for 27 h. It is obvious that the interface between the bond-coat and matrix is still observable, indicating the matrix has not been severely oxidized. In Fig. 5, a microcrack can be seen at/near the interface between the bond-coat

and top-coat. In the low magnification OM image, we can see that this kind of micro-crack was discontinuous and wavy and did not grow larger, even after 240 h oxidation at 1000°C. Therefore, the top-coat of the APS specimen was not observed to spall off even after 1000°C × 240 h oxidation.

Fig. 6(a) illustrates the 1000°C static oxidation test results of weight gain vs. oxidation time for APS-coated and un-coated specimens. Fig. 6(b) gives the same data as shown in Fig. 6(a), but expressed in terms of log–log scale. As seen from Fig. 6(a), the improvement of oxidation resistance on APS-coated Ti–48Al–2Cr–2Nb alloy is significant. Both weight gain and oxidation rate of APS-coated alloy are inhibited. The weight gain in Fig. 6 can be expressed by a kinetic power law:

$$\Delta w = k_i t^{n_i} \quad (1)$$

where Δw = weight gain (mg cm^{-2}); k_i = rate constant, here, k_1 is for the un-coated alloy, and k_2 is for the APS-coated alloy; t = oxidation time (s); n_i = index of oxidation rate, here, n_1 is for the un-coated alloy, n_2 is for the coated alloy n_i and k_i can be obtained by plotting log–log scale from Eq. (1), as shown in Fig. 6(b). It is significant for the APS-coated sample that both k_i and n_i are reduced, i.e., $n_1 = 0.291$ is reduced to $n_2 = 0.269$, and $k_1 = 0.2214$ is reduced to $k_2 = 0.1263$. This fact indicates that Ti–48Al–2Cr–2Nb alloy is effectively protected by the APS coating layers. Further discussion will be presented in Section 3.3 and Section 3.4.

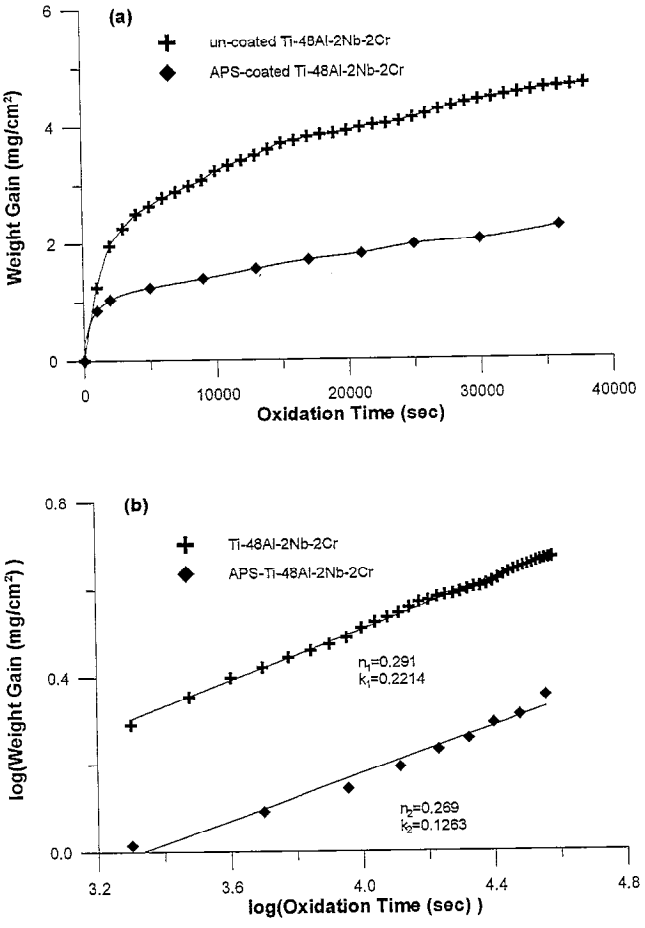

Fig. 6. (a) Weight gain vs. time of static oxidation tests both for the un-coated and coated specimens oxidized in air at 1000°C. (b) Log–log scale of (a).

3.2.2. *Cyclic oxidation test*

Fig. 7 demonstrates the results of weight gain vs. cyclic numbers of thermal cyclic oxidation tests for APS-coated Ti–48Al–2Cr–2Nb alloy. The thermal sequence of each cycle is also illustrated in the inset of Fig. 7. The data points of Fig. 7 were taken for every five thermal cycles during the cyclic testing course. From Fig. 7, the APS-coated specimen also shows a power curve during the thermal cyclic test, which is similar to the oxidation curve during the static oxidation test shown in Fig. 6(a). No weight loss or zigzag curve is observed in the data points of Fig. 7. This indicates that the oxide scale did not spall off during the dynamic thermal cycles of room and elevated temperatures; i.e., the APS-coated Ti–48Al–2Cr–2Nb has an excellent thermal cycling protection.

3.3. *Formation of oxidation layer in the oxidized Ni–4.5wt.%Al bond coat*

XRD analysis was utilized to investigate the oxide scale of APS-coated specimens which is gradually formed after the static oxidation at 1000°C. Fig. 8 shows the progressive XRD spectra taken from the bond-coat layer by polishing away the top-coat layer after specimens were oxidized at 1000°C. In Fig. 8, the main intensity peaks identified are NiO, and they grew rapidly with various oxidation times, e.g., 0, 5, 27 and 240 h. Note there is no other new phase formed. Fig. 9(a) and Fig. 9(b) show SEM images of oxidized APS-coated

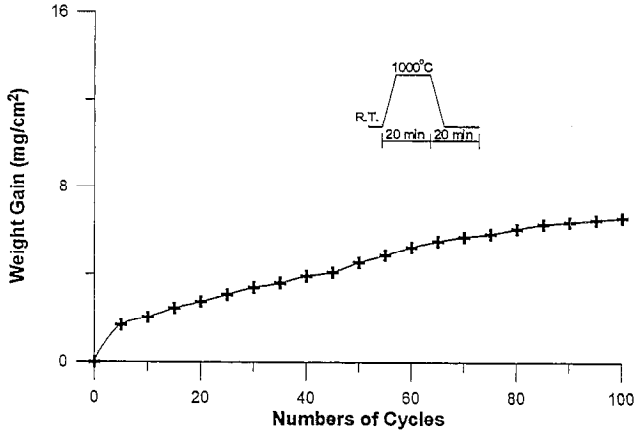

Fig. 7. Weight gain vs. number of cycles of the thermal cyclic oxidation test for the APS-coated specimen.

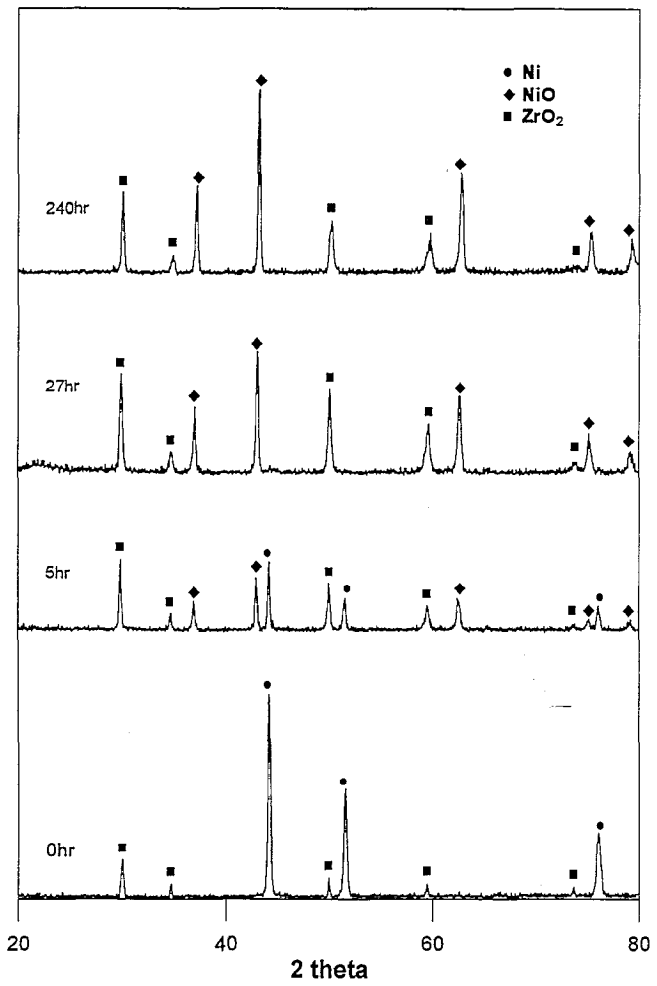

Fig. 8. Progressive XRD spectra of the oxidized bond-coat, showing the monotonic growth of NiO peaks as a function of oxidation time.

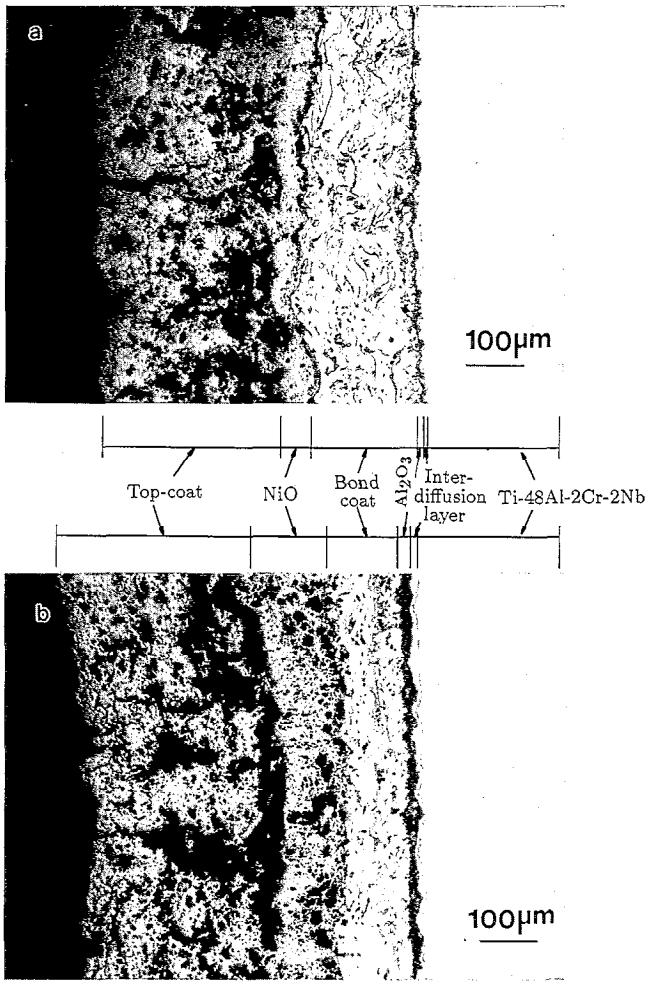

Fig. 9. OM microstructure of the APS-coated Ti–48Al–2Cr–2Nb specimens oxidized in air at 1000°C (a) for 27 and (b) for 240 h. Note the growth of NiO and Al_2O_3 layers.

Ti–48Al–2Cr–2Nb alloy oxidized at 1000°C for 27 and 240 h, respectively. As illustrated in Fig. 9(a) and Fig. 9(b), the Ni–4.5wt.%Al bond-coat now formed four layers, including a NiO scale, an unoxidized bond-coat, an Al_2O_3 layer and a Ti–Al–Ni inter-diffusion layer. The thicknesses of the NiO scale and the Al_2O_3 layer increased with increasing oxidation time.

In order to verify the performance of oxidation protection in the bond-coat, corresponding specimens from Fig. 9(a) and Fig. 9(b) with EPMA images and Ni, Al, Ti, O mappings were conducted at the interface between the bond-coat and matrix, and the results are shown in Fig. 10(a) and Fig. 10(b), respectively. From Fig. 10, three points can be made. (1) Some intermetallic phases do exist at the interface between bond-coat and matrix, presumably due to the inter-diffusion of titanium and nickel. This is the Ti–Al–Ni inter-diffusion layer, as shown in Fig. 9 and Fig. 10. Based on the EPMA quantitative analysis, it can be seen that the composition in this layer is 56.6%Ti+22.8%Al+20.6%Ni (all atomic percent) for the 27-h oxidation sample of Fig. 9(a) and Fig. 10(a), while it is 56.6%Ti+21.9%Al+21.5%Ni for the 240-h oxidation sample of Fig. 9(b) and Fig. 10(b). This fact indicates that nickel atoms diffused into this layer but aluminum and titanium atoms diffused out gradually as the oxidation time increased. Compared with the results shown in the Ti–Al–Ni ternary phase diagram [17], this inter-diffusion layer can be composed of $AlTi_3(\eta)+AlTiNi(\lambda)+NiTi_2$. These new intermetallic phases may improve bonding strength, but it is difficult to predict their influence on the oxidation resistance. (2) During oxidation, nickel plays the role of oxygen accepter by forming a NiO scale grown on the outer surface of the bond-coat. At the same time, aluminum acts in the role of oxygen inhibitor by forming an Al_2O_3 layer, grown in between the unoxidized bond-coat and the Ti–Al–Ni inter-diffusion layer. It is observed from EPMA mapping of Fig. 10(a) that Al_2O_3 was not distributed uniformly for the 27-h samples. However, a continuous and densified Al_2O_3 layer of about 20 μm in thickness was formed for the

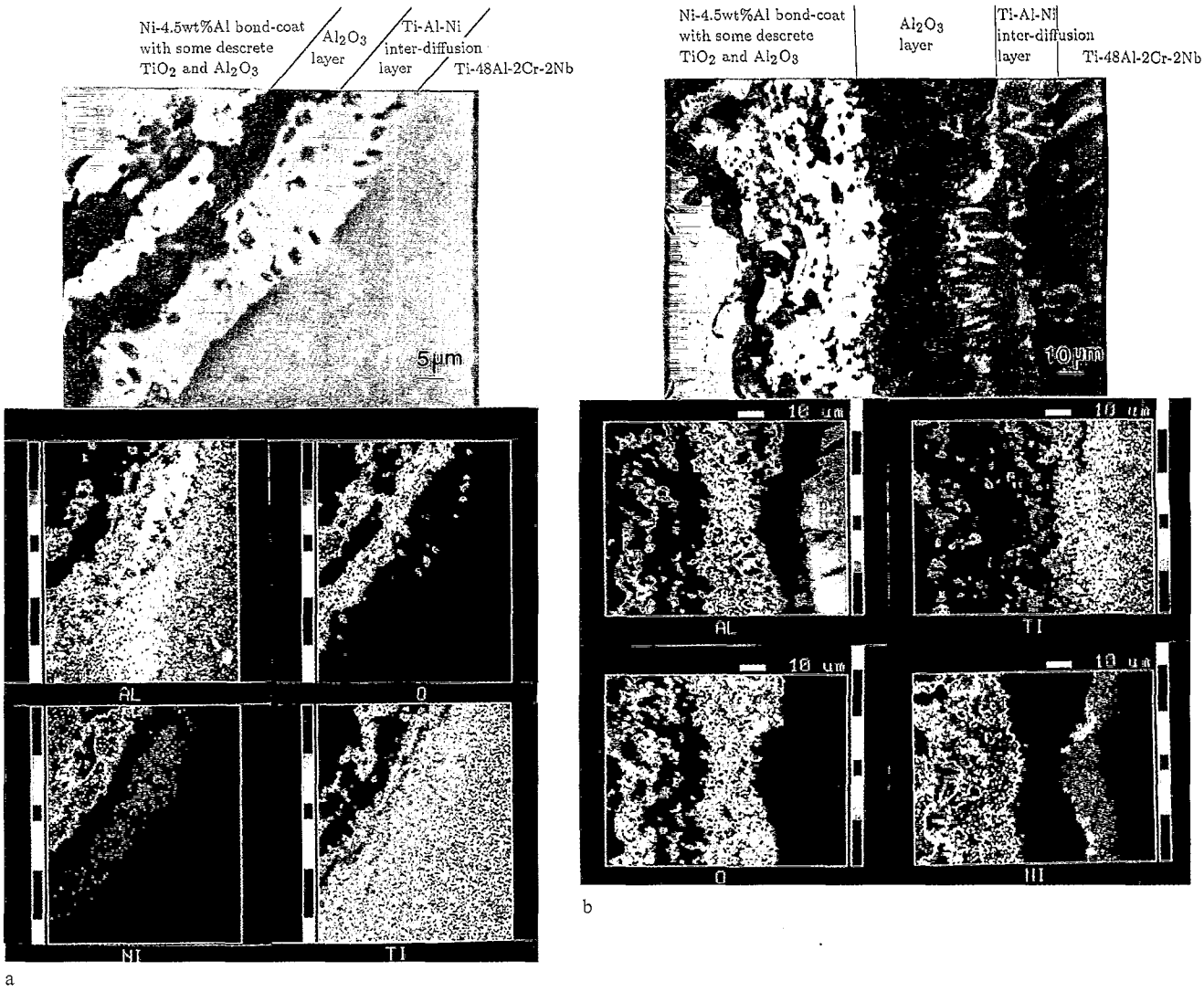

Fig. 10. SEM microstructure and EPMA Ti, Ni, Al, O mappings at the interface of bond-coat and matrix. Specimens were oxidized in air at 1000°C (a) for 27 h and (b) for 240 h.

240-h samples, as shown in Fig. 10(b). Virtually, the dense Al_2O_3 layer not only inhibits the inward oxygen diffusion but also prevents outward titanium diffusion. This implies that the oxidation resistance can be improved. (3) There are dilute particles of Al_2O_3 and TiO_2 loosely distributed in the bond-coat between outer NiO scale and inner Al_2O_3 layer, but there seems to be no significant influence on the bonding strength, nor does it seem to be a detriment to the oxidation performance.

3.4. Oxidation protection mechanism of APS-coated Ti–48Al–2Cr–2Nb alloy

From the experimental results of Fig. 8, Fig. 9, and Fig. 10, the mechanism of oxidation protection of APS-coated Ti–48Al–2Cr–2Nb alloy can be postulated. During oxidation at high temperature, oxygen permeates through the top-coat ZrO_2 pores to react with the bond-coat to form NiO scale on the outer surface of bond coat. Basically, NiO is not a good oxidation healing agent [16], however, it accumulates continuously as an oxygen accepter and delays the oxidation rate. Small amounts of oxygen can permeate the NiO scale to react with the unoxidized bond-coating causing some discrete TiO_2 and Al_2O_3 particles in this unoxidized layer. Experimental results show that TiO_2 and Al_2O_3 particles have a denser distribution at the innermost area of unoxidized bond-coat layer. This may be due to the fact that the APS bond-coat layer also has the same existing porosity, as was observed in the APS MCrAlY bond-coat layer [18]. At the same time, the bond-coat layer near the Ti–48Al–2Cr–2Nb substrate should have a high content of aluminum due to the outward diffusion of aluminum from the substrate during the 1000°C oxidation. This higher aluminum content layer will

favor Al_2O_3 formation on the inner layer of the bond-coat and act as a barrier to prevent oxygen from further permeation. Consequently, the rate of weight gain increases quickly at the beginning and then slows down because of the formation of an Al_2O_3 healer and the steady growth of the NiO scale, as shown in Fig. 6, Fig. 9, and Fig. 10.

The experimental results in Fig. 6 show that the oxidation kinetics of the APS-coated titanium aluminide alloys do not obey the parabolic law. For most metals and alloys, the oxidation kinetics follow the parabolic law ($n_i = 0.5$ in Eq. (1)) when the scale formation rate is determined by the reactant diffusion in the oxide scale. However, in this study, the index of oxidation rate, $n_1 = 0.291$, for the un-coated titanium aluminide alloy reduces to $n_2 = 0.269$ for the APS-coated one. This fact manifests that the oxidation in the bond-coat (as shown in Fig. 8) is not controlled solely by the transport process of metallic ions, but simultaneously healed by the formation of an Al_2O_3 layer.

4. Conclusions

(1) A top-coat of ZrO_2–8wt.%CaO together with a bond-coat of Ni–4.5wt.%Al can be effectively coated on the surface of Ti–48Al–2Cr–2Nb intermetallic compound by APS. Mechanical bonding strength between each coating and matrix is quite good. The hardness of the APS coating is significantly improved by ZrO_2 coating, almost doubled in comparison with the titanium aluminide intermetallic matrix.

(2) Both static and thermal cyclic oxidation tests show that the oxidation resistance of APS-coated Ti–48Al–2Cr–2Nb was improved. Experimental results show the oxidation kinetics of APS-coated titanium aluminide alloys does not obey the parabolic law, the index of oxidation rate in kinetic power law, $\Delta w = k_i t^{n_i}$, reduces from $n_i = 0.291$ for the un-coated sample to $n_i = 0.269$ for the APS-coated one. The improvement of oxidation resistance is attributed to the bond-coat of Ni–4.5wt.%Al.

(3) Through EPMA mapping and quantitative analysis for 1000°C oxidized samples, it is observed that the microstructure of the Ni–4.5wt.%Al bond-coat changed as a function of oxidation time. A NiO scale grows on the outer surface of the bond-coat, while an Al_2O_3 layer grows on the inner layer of the bond-coat. A Ti–Al–Ni intermetallic inter-diffusion zone exists, which is composed of $AlTi_3(\eta) + AlTiNi(\lambda) + NiTi_2$ phases. These new phases may improve bonding strength, but it is difficult to predict their influence on the oxidation resistance.

(4) The mechanism of oxidation protection of APS-coated Ti–48Al–2Cr–2Nb alloy can be proposed as following: during the oxidation at high temperature, oxygen permeates through the top-coat ZrO_2 pores to react with the bond-coat to form the NiO scale on the outer surface of the bond-coat. Small amounts of oxygen permeate through the NiO scale to react with aluminum and titanium to form TiO_2 and Al_2O_3 discretely distributed in the unoxidized bond-coat layer. A dense Al_2O_3 layer eventually forms on the inner layer of the bond-coat preventing ingress of oxygen.

Acknowledgement

The authors are grateful to Professor S.E. Hsu, Institute of Materials Science and Engineering, National Taiwan University, for his critical reading of the manuscript and helpful discussion. Also, they would like to thank Dr. J.Y. Wang, Materials R&D Center, Chung-Shan Institute of Science and Technology, Longtan, Taiwan, for his kind permission to use the JEOL JXA-8621MX EPMA. The financial support of this study by the National Science Council (NSC), Republic of China, under Grant NSC82-0405-E002-402 is also sincerely appreciated.

References

[1] H.A. Lipsitt, *Proc. Mater. Res. Soc., 39* (1985) 315–364.
[2] Y.W. Kim, *JOM, 41* (1989) 24–30.
[3] Y.W. Kim and D.M. Dimiduk, *JOM, 43* (1991) 40–47.
[4] Y. Umakoshi, M. Yamaguchi, T. Sakagami and T. Yamana, *J. Mater. Sci., 24* (1989) 1599.
[5] S. Taniguchi, *Bull. Jpn. Inst. Metals, 31* (1992) 497. (In Japanese).
[6] G.E. Fuchs, *Proc. ISSI Structural Intermetallics*, TMS, 1993, pp. 195–203.
[7] S.C. Huang and E.L. Hall, *Metall. Trans. A, 22A* (1991) 2619–2627.
[8] R. Sivakumar and B.L. Mordike, *Surf. Eng., 2* (1988) 127–140.
[9] K. Takeda, K. Hayashi and T. Ohashi, *Proc. ISPC-7*, 1985, p. 810.
[10] K. Takeda, M. Ito and S. Takeuchi, *Pure Appl. Chem., 67* (1990) 1773.
[11] S. Sacre, *Surf. Coat. Technol., 67* (1994) 9–15.
[12] G. Johner and K.K. Schweitzer, *Thin Solid Films, 95* (1982) 265.
[13] T.E. Strangeman, *Thin Solid Films, 119* (1984) 301.
[14] S.M. Meier, D.K. Gupta and D. Sheffler, *JOM, March* (1991) 50–53.
[15] A. Bennett, *Surf. Coat. Technol., 32* (1987) 359.
[16] C.C. Young, L.C. Chen, S. Torng and S.E. Hsu, *The 6th Asian-Pacific Corrosion Conference*, 1989, pp. 16–25.
[17] K.J. Lee and P. Nash, *J. Phase Equilibria, 12(5)* (1991) 551–562.
[18] P.Y. Pekshev and I.G. Murzin, *Surf. Coat. Technol., 56* (1993) 199–203.